

DEATH LINE OF GAMMA-RAY PULSARS WITH OUTER GAPS

REN-BO WANG¹

Department of Physics, National Dong Hwa University, Hualien 97401, Taiwan

AND

KOUICHI HIROTANI²

Theoretical Institute for Advanced Research in Astrophysics (TIARA), Academia Sinica, Institute of Astronomy and Astrophysics (ASIAA), PO Box 23-141, Taipei, Taiwan

accepted 2011 May

ABSTRACT

We analytically investigate the condition for a particle accelerator to be active in the outer magnetosphere of a rotation-powered pulsar. Within the accelerator (or the gap), magnetic-field-aligned electric field accelerates electrons and positrons, which emit copious gamma-rays via curvature process. If one of the gamma-rays emitted by a single pair materializes as a new pair on average, the gap is self-sustained. However, if the neutron-star spin-down rate decreases below a certain limit, the gap becomes no longer self-sustained and the gamma-ray emission ceases. We explicitly compute the multiplicity of cascading pairs and find that the obtained limit corresponds to a modification of previously derived outer-gap death line. In addition to this traditional death line, we find another death line, which becomes important for millisecond pulsars, by separately considering the threshold of photon-photon pair production. Combining these traditional and new death lines, we give predictions on the detectability of gamma-ray pulsars with Fermi and AGILE. An implication on the X-ray observations of heated polar-cap emission is also discussed.

Subject headings: gamma rays: stars — magnetic fields — methods: analytical — stars: neutron

1. INTRODUCTION

The *Fermi* Large Area Telescope (LAT) provides a wealth of new data on isolated, rotation-powered pulsars, increasing the number of detected γ -ray pulsars from seven to more than sixty (e.g., Abdo et al. 2010a). The *AGILE* has also reported the detection of about twenty γ -ray pulsars (e.g., Pellizzoni et al. 2009). Since interpreting γ -rays should be less ambiguous compared with reprocessed, non-thermal X-rays, the γ -ray pulsations observed from these objects are particularly important as a direct signature of basic non-thermal processes in pulsar magnetospheres, and potentially should help to discriminate among different emission models.

In a pulsar magnetosphere (fig. 1), there is a surface called the ‘null surface’, on which the Goldreich-Julian charge density (Goldreich & Julian 1969) $\rho_{\text{GJ}} \equiv \mathbf{B} \cdot \boldsymbol{\Omega} / (2\pi c)$ changes sign, where \mathbf{B} denotes the local magnetic field, $\boldsymbol{\Omega}$ the NS angular-velocity vector, and c the speed of light. There is another characteristic surface called the ‘light cylinder’ beyond which the co-rotational velocity exceeds c . The distance of the light cylinder from the rotation axis is called the ‘light-cylinder radius’, $\varpi_{\text{LC}} \equiv c/\Omega$, where $\Omega \equiv |\boldsymbol{\Omega}|$ denotes the NS rotational angular frequency. On each magnetic azimuthal angle (measured around the magnetic axis), there is a magnetic field line that crosses the light cylinder tangentially; they are called the ‘the last-open field lines’.

In the lower colatitudes than the last-open field lines,

field lines closes inside the light cylinder; thus, a high plasma density is expected by the trapping of relativistic charges due to magnetic mirrors, preventing the occurrence of a strong magnetic-field-aligned electric field, E_{\parallel} , in this closed zone. In the higher colatitudes, on the other hand, field lines open to a distant region beyond the light cylinder, allowing a pulsar wind to flow along them, thereby resulting in a high vacuum with unscreened E_{\parallel} in some regions in this open-field-line zone.

On these grounds, in all the pulsar emission models, particle acceleration is assumed to realize in the open zone. In polar-cap (PC) models, emission takes place within a few neutron star (NS) radii above a PC surface (Arons & Scharlemann 1979; Daugherty & Harding 1982, 1996). However, the observed cutoff energies, typically between 1 GeV and 4 GeV (Abdo et al. 2010a), along with the 25 GeV detection of pulsed signals from the Crab pulsar (Aliu et al. 2008), suggests no attenuation from one-photon absorption by a strong magnetic field (Baring 2004) near the NS, indicating the minimum altitudes of a few stellar radii above the PC surface. Thus, the possibility of a high-altitude emission gathered attention.

Recent pulsar high-energy emission models adopt, therefore, higher-altitude geometries. There are two main scenarios in this approach: the outer-gap (OG) model (Cheng et al. 1986a, b; Romani 1996; Cheng et al. 2000; Hirotani 2008; Takata et al. 2008; Romani & Watters 2010), and the pair-starved polar-cap model (Frackowiak & Rudak 2005; Harding et al. 2005; Venter et al. 2009).

In the present paper, we focus on the OG model, in which pairs are created in the outer magnetosphere mainly by photon-photon (γ - γ) pair production. The

Electronic address: rbwang1225@gmail.com
Electronic address: hirotani@tiara.sinica.edu.tw

¹ Summer student of ASIAA in 2010

² Postal address: TIARA, Department of Physics, National Tsing Hua University, 101, Sec. 2, Kuang Fu Rd., Hsinchu, Taiwan 300

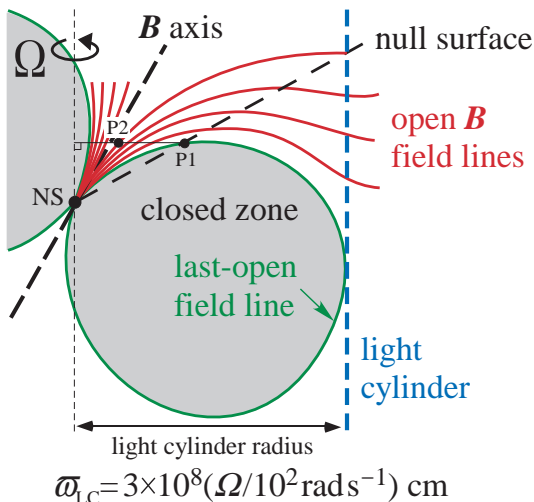


FIG. 1.— Side view of magnetic field lines on the meridional plane in which both the magnetic and rotational axes reside.

produced pairs polarize owing to the magnetic-field-aligned electric field, E_{\parallel} . If the rotation and magnetic axes reside in the same hemisphere, a positive E_{\parallel} is exerted to accelerate e^{+} 's (or e^{-} 's) outward (or inwards), increasing the real charge density outwards. The inward-migrating, relativistic e^{-} 's radiate curvature γ -rays, some of which (nearly head-on) collide with the X-rays emitted from the NS surface to materialize as pairs.

The purpose here is to examine the detectability of the γ -ray photons from pulsars with OG accelerators. On the neutron-star period (P) versus period-derivative (\dot{P}) plane, we find two kinds of death lines below which the pulsar OGs become inactive. In § 2, we derive the first kind death line, which turns out to be a modification of the previous death lines (Zhang et al. 2004). We then derive the second kind, new death line in § 3, by separately considering the threshold of γ - γ pair production. We finally combine these two death lines and discuss the detectability of pulsars with recent γ -ray telescopes.

2. DEATH LINE DERIVED BY MULTIPLICITY CONSTRAINT

According to the analytical consideration in classic OG model (Cheng et al. 1986a, b; Romani 1996; Cheng et al. 2000), and to the numerical solution of the OG (Hirotani 2006a,b), an OG is found to exist essentially between the null surface and the light cylinder (fig. 1). Since most of the pairs are produced in the inner-most region of the OG, the (outward-moving) e^{+} 's propagate longer distance than the (inward-moving) e^{-} 's. As a result, the outward γ -ray flux becomes greater than the inward one. This result is particularly important when we predict the high-energy emission properties from an OG. Nevertheless, to investigate the condition for an OG to be self-sustained, it is crucial to consider the collisions between the *inward* γ -rays, which are emitted by e^{-} 's, and the outward-propagating X-rays, which are emitted from the heated PC surface. Thus, in this paper, we concentrate on the condition for the inward-propagating γ -rays to materialize as pairs in the inner magnetosphere.

For young pulsars like Crab or Vela, γ - γ pair production is sustained by the strong thermal emission from the cooling NS surface, and the gap trans-field thickness is

kept thin. However, as the NS ages, the heated PC emission due to the bombardment of in-falling e^{-} 's dominates the cooling NS emission and controls the gap trans-field thickness. Therefore, when we investigate the death lines below which an OG accelerator ceases to emit γ -rays, it is appropriate to consider the heated PC as the source of X-rays for γ - γ pair production. For simplicity, we assume that the heated PC has a uniform temperature kT with area πR_{pc}^2 . When the OG activity is marginally sustained, pair production takes place mainly near the null surface.

2.1. Optical depth of photon-photon pair production

At an altitude $r - r_* \gg R_{\text{pc}}$, the photon energy flux is given by

$$F = F_* \left(\frac{R_{\text{pc}}}{r - r_*} \right)^2 \cos \Theta, \quad (1)$$

where the flux measured at the surface becomes

$$F_* = 1.0 \times 10^{20} \left(\frac{kT}{100 \text{ eV}} \right)^4 \text{ erg s}^{-1} \text{ cm}^{-2}; \quad (2)$$

r_* denotes the NS radius, Θ the colatitude of the point from the *magnetic* axis. In this paper, we consider that the magnetic axis is moderately or highly inclined with respect to the rotation axis. In this case, the PC surface is almost face-on from the gap inner boundary, which is located well inside the light cylinder. Thus, we adopt $\cos \Theta \approx 1$ in what follows.

Evaluating the photon number flux at typical blackbody photon energy, $h\nu_x \approx 2.8kT$, we obtain the mean-free path for an inward-propagating γ -ray to materialize in a collision with the surface X-ray as

$$\begin{aligned} \lambda_p &= \left(\frac{1}{c} \frac{F}{h\nu_x} \right)^{-1} \sigma_p^{-1} \\ &\approx 9.9 \times 10^5 \left(\frac{kT}{100 \text{ eV}} \right)^{-3} \left(\frac{r - r_*}{R_{\text{pc}}} \right)^2 \text{ cm}, \end{aligned} \quad (3)$$

where the γ - γ pair-production total cross section is evaluated by $\sigma_p \sim 0.2\sigma_T = 1.3 \times 10^{-25} \text{ cm}^2$, because the collisions take place mostly head-on.

Inward-propagating γ -rays are typically emitted from the central colatitude in the gap. Therefore, before crossing the critical field lines on which the null surface intersects the light cylinder (i.e., before escaping from the gap), they propagate the distance

$$l \approx \frac{r_{\text{null}}}{\sqrt{2}} (\sin \theta_{\text{null}} - \tan \alpha \cos \theta_{\text{null}}), \quad (4)$$

where r_{null} denotes the distance of the null surface on the last-open field line from the NS center, α the angle between rotation and magnetic axes. If $\alpha = 75^\circ$, $\theta_{\text{null}} \approx 85^\circ$ gives $l \approx 0.67r_{\text{null}}$, whereas if $\alpha = 45^\circ$, $\theta_{\text{null}} \approx 74^\circ$ gives $l \approx 0.47r_{\text{null}}$, for example. Note that the gap is supposed to exist only below the critical field lines, because such solutions are being obtained by three-dimensional OG simulations. Because of this geometry, the obtained death lines give tighter constraints than previous ones, which are obtained by assuming that the OG occupies the entire open-field-line regions between the null surface and the light cylinder (i.e., by imposing $f < 1$ as in Zhang et al. 2004).

Combining equations (3) and (4), we can compute the optical depth $\tau = l/\lambda_p$ for γ - γ pair production,

$$\tau \approx 1.0 \left(\frac{kT}{100 \text{ eV}} \right)^3 \left(\frac{R_{\text{pc}}}{r_*} \right)^2 \frac{\eta}{(\eta - 1)^2} r_{*,6} \frac{l}{r_{\text{null}}}, \quad (5)$$

where $\eta \equiv r/r_*$, $r_{*,6} \equiv r/(10^6 \text{ cm})$, $P = 2\pi/\Omega$ is the NS spin period; $r \approx r_{\text{null}}$ is used.

2.2. Acceleration electric field

For the pulsars near the death line (to be derived below), the potential drop in the OG becomes a good fraction of the electromotive force, $V_* \approx B_* r_*^3 / (2\varpi_{\text{LC}}^2)$, exerted on the PC surface. Thus, we can reasonably evaluate the maximally possible E_{\parallel} by

$$E_{\parallel} \approx \frac{0.5V_*}{\varpi_{\text{LC}}} \approx \frac{B_* r_*^3}{4\varpi_{\text{LC}}^3} = \frac{\mu}{2\varpi_{\text{LC}}^3}, \quad (6)$$

where μ denotes the NS dipole moment, and B_* the magnetic field strength at the NS surface. Since the potential drop occurs only in a portion of the open zone, we multiply the factor 0.5 in the numerator. By this acceleration electric field, the inward motion of e^- 's attain a force balance between the electrostatic and curvature-radiation forces. Thus, the typical Lorentz factors of the e^- 's become

$$\gamma = \left(\frac{3R_c^2}{2e} E_{\parallel} \right)^{1/4}, \quad (7)$$

where e refers to the magnitude of the charge on the electron, R_c the curvature radius of the magnetic field line.

2.3. Evaluation of curvature radius

To evaluate R_c , we consider the following two representative cases.

Case 1: The null surface intersects the last-open field line in the *inner-most* magnetosphere; that is, $r_{\text{null}} < 0.05\varpi_{\text{LC}}$. In this case, the curvature radius can be approximated as

$$R_c \approx \frac{4}{3} \sqrt{\frac{r}{\varpi_{\text{LC}}}} \varpi_{\text{LC}} \quad (8)$$

on the last-open field line. If $\alpha > 70^\circ$, this case becomes applicable along the magnetic field lines that crosses the NS surface with magnetic azimuthal angle in the range $-60^\circ < \varphi_* < 60^\circ$, where φ_* increases counter-clockwise and $\varphi_* = \pi$ points the rotation axis from the magnetic axis. To derive the OG death line, it is sufficient to consider only this range, $|\varphi_*| < 60^\circ$, because the OG is active only in $|\varphi_*| < 60^\circ$.

Case 2: The null surface intersects the last-open field line in the *outer* magnetosphere; that is, $r_{\text{null}} > 0.07\varpi_{\text{LC}}$. In this case, we have

$$R_c \approx 0.5\varpi_{\text{LC}}. \quad (9)$$

If $\alpha < 62^\circ$, this case becomes applicable in $|\varphi_*| < 60^\circ$.

2.4. Typical gamma-ray energies

Substituting equation (6) into (7), we obtain

$$\gamma \approx 3.3 \times 10^6 \eta^{1/4} P^{-1/2} \mu_{30}^{1/4} r_{*,6}^{1/4}, \quad (10)$$

for case 1, and

$$\gamma \approx 1.7 \times 10^7 P^{-1/4} \mu_{30}^{1/4}, \quad (11)$$

for case 2, where $\mu_{30} = \mu/(10^{30} \text{ G cm}^3)$.

The flux density of the curvature spectrum peaks at the frequency $0.29\nu_c$, where the critical frequency is defined by

$$\nu_c \equiv \frac{3c\gamma^3}{4\pi R_c}. \quad (12)$$

However, for the pulsars near the death line, γ - γ pair production is maintained by the collisions between the γ -ray photons with energy $h\nu_\gamma \gg 0.29h\nu_c$ and the thermal photons near the blackbody peak $h\nu_s \sim 2.82kT$, or between the γ -rays with $h\nu_\gamma \sim 0.29h\nu_c$ and the thermal photons in the Wien regime $h\nu_s \gg 2.82kT$, or both (i.e., $h\nu_\gamma > 0.29h\nu_c$ and $h\nu_s > 2.82kT$). To take account of such effects, we can practically assume that pair production takes place between the γ -rays with $h\nu_\gamma \sim h\nu_c$ and the surface X-rays with $h\nu_s \sim 3kT$; this treatment incurs relatively small errors from the exact, complicated numerical computations.

Substituting equations (10) or (11) into (12), we obtain the typical γ -rays energy,

$$h\nu_c = 11.8 \eta^{1/4} P^{-2} \mu_{30}^{3/4} r_{*,6}^{1/4} \text{ MeV}, \quad (13)$$

$$h\nu_c = 60 P^{-7/4} \mu_{30}^{3/4} \text{ MeV} \quad (14)$$

for cases 1 and 2, respectively.

2.5. Number of gamma-rays emitted by each electron

Let us now evaluate number of photons emitted by a single inward-accelerated e^- near the null surface, the inner-most region of the gap. If R_c were constant in the magnetosphere, the photons emitted between the altitudes r_{null} and $(r_{\text{null}} + l)$ illuminate the null surface, where l is given by equation (4). Therefore, we could evaluate the number of γ -rays emitted by a single e^- by

$$N_\gamma \approx \frac{eE_{\parallel}l}{h\nu_c}. \quad (15)$$

It follows that a single e^- cascade into $N_\gamma\tau$ secondary pairs within the gap.

Substituting equations (13) or (14) into (15), we obtain

$$N_\gamma \approx 78 \eta^{3/4} P^{-1} \mu_{30}^{1/4} r_{*,6}^{3/4} \frac{l}{0.67r_{\text{null}}}, \quad (16)$$

$$N_\gamma \approx 10.8 \eta P^{-5/4} \mu_{30}^{1/4} r_{*,6} \frac{l}{0.47r_{\text{null}}} \quad (17)$$

for cases 1 and 2, respectively.

2.6. Number of secondary pairs cascaded from a primary electron

Combining equations (5) and (16), we obtain the number of pairs that a single e^- cascades within the gap,

$$N_\gamma\tau \approx 52 \frac{\eta^{7/4}}{(\eta - 1)^2} \left(\frac{R_{\text{pc}}}{r_*} \right)^2 \left(\frac{kT}{100 \text{ eV}} \right)^3 \times P^{-1} \mu_{30}^{1/4} r_{*,6}^{7/4} \left(\frac{l}{0.67r_{\text{null}}} \right)^2 \quad (18)$$

for case 1. In the same manner, combining equations (5) and (17), we obtain

$$N_{\gamma}\tau \approx 5.0 \frac{\eta^2}{(\eta-1)^2} \left(\frac{R_{\text{pc}}}{r_*}\right)^2 \left(\frac{kT}{100 \text{ eV}}\right)^3 \times P^{-5/4} \mu_{30}^{1/4} r_{*,6}^2 \left(\frac{l}{0.47 r_{\text{null}}}\right)^2 \quad (19)$$

for case 2. We have to express $(R_{\text{pc}}/r_*)^2$ so that the emitted energy in the form of the blackbody radiation from the heated PC surface may be consistent with the energy deposited by the bombardment of gap-accelerated e^- 's.

2.7. Effective area of heated polar-cap

The number flux of e^- 's falling onto the polar cap surface (with area A_{gap}) can be evaluated by

$$\dot{N}_e = \kappa \frac{\Omega B_*}{2\pi e} A_{\text{gap}} \approx 5.5 \times 10^{29} \kappa P^{-2} \mu_{30} \frac{A_{\text{gap}}}{0.2 A_{\text{open}}}, \quad (20)$$

where $A_{\text{open}} \sim \pi r_*^3 / \varpi_{\text{LC}}$ denotes the entire PC area. Since typically 20% of the open flux tubes thread the gap, $A_{\text{gap}} \sim 0.2 A_{\text{open}}$ is a good compromise. See figure 3 for an example of active field lines on the PC surface, which indicates that about 20% of the open field line fluxes are active.

From numerical analysis, $\kappa \sim 0.3$ is appropriate for $\alpha \sim 75^\circ$, while $\kappa \sim 0.7$ for $\alpha \sim 45^\circ$. In Newtonian approximation, κ typically becomes $\cos \alpha$, because we obtain $B_z/B = \cos \alpha$ at the PC surface, where B_z refers to the magnetic field component projected along the rotation axis. Thus, κ decreases with increasing α . However, as the NS rapidly rotates, the space-time dragging effect (Muslimov & Tsygan 1992) leads to a smaller κ than $\cos \alpha$. On the other hand, in a three-dimensional pulsar magnetosphere, inward γ -rays preferentially propagates towards the leading side due to the aberration of the photon propagation direction; thus, created current becomes super Goldreich-Julian in the leading side to exert a space-charge-limited flow of ions from the PC surface in an OG (H06a). Thus, κ can exceed the value $\rho_{\text{GJ}}/(\Omega B/2\pi e)$ at the PC surface. For a highly inclined case, the fraction of the field lines having super-Goldreich-Julian current density increases because of the decreased ρ_{GJ} at the PC surface. Thus, $\kappa \sim 0.3$ is more appropriate than $\cos(75^\circ) = 0.26$ for $\alpha = 75^\circ$. However, for $\alpha = 45^\circ$, most field lines have sub-Goldreich-Julian current; thus, we obtain $\kappa \approx \cos(45^\circ) = 0.70$. As an intermediate case, we present the solution of κ in a three-dimensional OG with $\alpha = 60^\circ$ in the left panel of figure 3, which shows that the evaluation of $\kappa \approx \cos(60^\circ) = 0.5$ is appropriate on average.

Each e^- brings the energy $\gamma_{\text{h}} m_e c^2$ on the NS surface, where γ_{h} denotes the Lorentz factor at the altitude $r = r_{\text{h}} \equiv \sqrt{2r_* \varpi_{\text{LC}}}$ below which all the emitted photons hit the NS. For case 1, most of the e^- 's kinetic energy at the gap inner boundary will be eventually turned into the NS surface emission, because $r_{\text{h}}/\varpi_{\text{LC}} \approx 0.028 \sqrt{r_{*,6}/P}$ shows that $r_{\text{null}} < r_{\text{h}}$ if $P < 0.3$ s. For case 2, on the contrary, only a portion of $\gamma m_e c^2$ at the null surface will

be used in the heating of the NS surface, because $r_{\text{null}} > r_{\text{h}}$.

For case 1, we can put $\gamma_{\text{h}} = \gamma$, where the right-hand side is evaluated by equation (10). Thus, combining equations (10) and (20), we obtain

$$\gamma_{\text{h}} m_e c^2 \dot{N}_e \approx 4.5 \times 10^{29} \eta^{1/4} P^{-5/2} \mu_{30}^{5/4} \times r_{*,6}^{1/4} \frac{\kappa}{0.3} \frac{A_{\text{gap}}}{0.2 A_{\text{open}}} \text{ erg s}^{-1}. \quad (21)$$

For case 2, on the other hand, electrons lose energy by curvature radiation from $r = r_{\text{null}}$ down to $r = r_{\text{h}}$ before illuminating the NS. Integrating the equation of Lorentz factor evolution,

$$\frac{d\gamma}{dt} m_e c^2 = \frac{2e^2}{3R_c^2} \gamma^4 \quad (22)$$

from $r = r_{\text{null}}$ to $r = r_{\text{h}}$, we obtain

$$\gamma_{\text{h}} \approx 2.5 \times 10^7 P^{1/3} \left[\ln \left(\frac{r_{\text{null}}}{r_{\text{h}}} \right) \right]^{-1/3} \quad (23)$$

where the weak dependence on $r_{\text{null}}/r_{\text{h}}$, which is of the order of unity, may be neglected. Combining equations (23) and (20), we obtain

$$\gamma_{\text{h}} m_e c^2 \dot{N}_e \approx 7.8 \times 10^{30} P^{-5/3} \mu_{30} \times \frac{\kappa}{0.7} \frac{A_{\text{gap}}}{0.2 A_{\text{open}}} \text{ erg s}^{-1}. \quad (24)$$

Equating the heating rate $\gamma_{\text{h}} m_e c^2 \dot{N}_e$ derived just above with the emission rate $\pi R_{\text{pc}}^2 \sigma T^4$, where σ denotes the Stefan-Boltzmann constant, we can evaluate the effective area of the heated PC region, πR_{pc}^2 , and obtain

$$\left(\frac{R_{\text{pc}}}{r_*}\right)^2 = 1.4 \times 10^{-3} P^{-5/2} \mu_{30}^{5/4} \times \left(\frac{kT}{100 \text{ eV}}\right)^{-4} \eta^{1/4} r_{*,6}^{-7/4} \frac{\kappa}{0.3} \frac{A_{\text{gap}}}{0.2 A_{\text{open}}} \quad (25)$$

for case 1, and

$$\left(\frac{R_{\text{pc}}}{r_*}\right)^2 = 2.4 \times 10^{-2} P^{-5/3} \mu_{30} \times \left(\frac{kT}{100 \text{ eV}}\right)^{-4} r_{*,6}^{-2} \frac{\kappa}{0.7} \frac{A_{\text{gap}}}{0.2 A_{\text{open}}} \quad (26)$$

for case 2. Note that $A_{\text{gap}}/A_{\text{open}}$ merely parametrizes the fraction of active field lines to the entire open field lines.

2.8. Multiplicity constraint

For case 1, substituting equation (25) into (18), we obtain

$$N_{\gamma}\tau \approx 6.3 \times 10^{-2} \left(\frac{\eta}{\eta-1}\right)^2 \left(\frac{kT}{100 \text{ eV}}\right)^{-1} \times P^{-7/2} \mu_{30}^{3/2} \frac{\kappa}{0.3} \frac{A_{\text{gap}}}{0.2 A_{\text{open}}} \left(\frac{l}{0.67 r_{\text{null}}}\right)^2. \quad (27)$$

For case 2, substituting equation (26) into (19), we obtain

$$N_{\gamma}\tau \approx 1.2 \times 10^{-1} \left(\frac{\eta}{\eta-1} \right)^2 \left(\frac{kT}{100 \text{ eV}} \right)^{-1} \times P^{-35/12} \mu_{30}^{5/4} \frac{\kappa}{0.7} \frac{A_{\text{gap}}}{0.2A_{\text{open}}} \left(\frac{l}{0.47r_{\text{null}}} \right)^2. \quad (28)$$

In this paper, we evaluate the NS magnetic moment assuming the vacuum dipole radiation formula, $\mu^2 = 3Ic^3 P \dot{P} / (8\pi^2)$. Then, equations (27) and (28) give

$$N_{\gamma}\tau \approx 7.4 \times 10^{-2} \left(\frac{\eta}{\eta-1} \right)^2 \left(\frac{kT}{100 \text{ eV}} \right)^{-1} I_{45}^{3/4} \times P^{-11/4} \dot{P}_{-15}^{3/4} \frac{\kappa}{0.3} \frac{A_{\text{gap}}}{0.2A_{\text{open}}} \left(\frac{l}{0.67r_{\text{null}}} \right)^2, \quad (29)$$

$$N_{\gamma}\tau \approx 1.2 \times 10^{-1} \left(\frac{\eta}{\eta-1} \right)^2 \left(\frac{kT}{100 \text{ eV}} \right)^{-1} I_{45}^{5/8} \times P^{-55/24} \dot{P}_{-15}^{5/8} \frac{\kappa}{0.7} \frac{A_{\text{gap}}}{0.2A_{\text{open}}} \left(\frac{l}{0.47r_{\text{null}}} \right)^2 \quad (30)$$

for cases 1 and 2, respectively.

Setting $N_{\gamma}\tau > 1$, we obtain the death line on the P versus \dot{P} plane, which describes the condition for an OG to emit γ -rays efficiently. Thus, the minimum spin-down rate for a given P is obtained as

$$\lg \dot{P} = -13.49 + 3.67 \lg P, \quad (31)$$

$$\lg \dot{P} = -13.54 + 3.67 \lg P \quad (32)$$

for cases 1 and 2, respectively.

Since we consider that the gap will not extend in the entire open field line region, the obtained death lines (31) and (32) gives a tighter constraint than previous works. For example, Zhang et al. (2004) gives

$$\lg \dot{P} = -14.60 + 3.33 \lg P \quad (33)$$

for a uniform distribution of α 's, and

$$\lg \dot{P} = -14.20 + 3.33 \lg P \quad (34)$$

for a cosine distribution of α . Death Lines (33) and (34) are depicted by the thick and thin dash-dotted lines in figure 2.

3. DEATH LINE DERIVED BY PAIR-PRODUCTION THRESHOLD

We now turn to the second and important constraint obtained by pair-production threshold. To derive this, we must evaluate the maximally possible energies of both the surface X-rays and the curvature γ -rays.

First, let us examine the maximum surface temperature, kT_{max} , which is probably realized in a limited area of the heated PC, near the footpoints of active magnetic field lines. That is, we release the assumption of uniform kT on the heated PC surface, which was adopted in § 2. Electrons will fall onto the NS surface with the typical Lorentz factor given by equation (23), where r_{h} may be replaced with r_* . However, the logarithmic factor little changes the right-hand side;

thus, we evaluate the Lorentz factor of in-falling e^- 's by $\gamma_7 = 2.5P^{1/3}$, where $\gamma_7 = \gamma/10^7$. Equating σT_{max}^4 with $\gamma m_e c^2 \dot{N}_e / A_{\text{gap}} = \gamma m_e c^2 \kappa \Omega B_*/(2\pi e)$, we obtain

$$kT_{\text{max}} = 426 \text{ eV} \kappa^{1/4} \gamma_7^{1/4} P^{-1/4} \mu_{30}^{1/4} r_{*,6}^{-3/4}. \quad (35)$$

Therefore, the typical X-ray energy can be estimated by

$$h\nu_X \approx 3kT_{\text{max}} \approx 0.0023 m_e c^2 \left(\frac{\kappa}{0.3} \right)^{1/4} P^{-1/6} \mu_{30}^{1/4} r_{*,6}^{-3/4} \quad (36)$$

for both case 1 and case 2, apart from the difference of κ .

Second, we examine the maximum energy of curvature photons. For case 1, we use equation (13) with $\eta = 2.4 \times 10^3 P(r/0.5\varpi_{\text{LC}})$ to obtain

$$h\nu_{\gamma} = 1.6 \times 10^2 m_e c^2 P^{-7/4} \mu_{30}^{3/4} r_{*,6}^{1/4}. \quad (37)$$

For case 2, we compute $h\nu_{\gamma}$ by equation (14).

Third, we impose the pair-production threshold condition, $h\nu_X \times h\nu_{\gamma} > (m_e c^2)^2$ to obtain

$$\lg \dot{P} = -14.15 + 2.83 \lg P, \quad (38)$$

$$\lg \dot{P} = -14.06 + 2.83 \lg P \quad (39)$$

for cases 1 and 2, respectively.

On these grounds, the actual death line is obtained by taking the greater \dot{P} in each case. For case 1, we obtain

$$\lg \dot{P} = \max(-13.49 + 3.67 \lg P, -14.15 + 2.83 \lg P), \quad (40)$$

and for case 2, we obtain

$$\lg \dot{P} = \max(-13.54 + 3.67 \lg P, -14.06 + 2.83 \lg P). \quad (41)$$

It follows that the death line little depends on α . In figure 2, the death line (40) is plotted as the (red) thick solid line. Case 2 (eq. [41]) is not plotted, because it almost overlaps on case 1 (eq. [40]). The (blue) squares denote the γ -ray detected pulsars, the (blue) triangles the millisecond γ -ray pulsars, and the (blue) circles other radio-loud γ -ray pulsars detected with Fermi and/or AGILE (Aliu et al. 2008; Halpern et al. 2008; Pellizzoni et al. 2009; Abdo et al. 2010a; Abdo et al. 2010b; Abdo et al. 2010c; Pilia et al. 2010; Saz Parkinson et al. 2010; Pilia & Pellizzoni 2011; Saz Parkinson et al. 2011; Guillemot et al. 2011; Keith et al. 2011). The (green) small open circles denotes the X-ray detected pulsars (see Grindlay and Bogdanov 2009, Becker & Trümper 1999, Becker 2009, for reviews; see also Grindlay et al. 2002, Bogdanov et al. 2006, Bogdanov et al. 2010, Bogdanov et al. 2011, Saito et al. 1997, Becker et al. 2003, Bassa et al. 2004, D'Amico et al. 2002, Elsner et al. 2008, and Heinke et al. 2006 for the millisecond pulsars in globular clusters; Kuiper et al. 2000, Mineo et al. 2000, Kuiper et al. 2002 for J0218+4232; Zavlin & Pavlov 1998, Zavlin et al. 2002 for J0437-4715; Bogdanov & Grindlay 2009 for J0030+0451; Zavlin 2006 for J0437-4715, J2124-3358, J1024-0719, J0034-0534). The small black dots denote radio pulsars that do not show either γ -ray or X-ray pulsations (ATNF pulsar catalog³).

³ <http://www.atnf.csiro.au/research/pulsar/psrcat/>

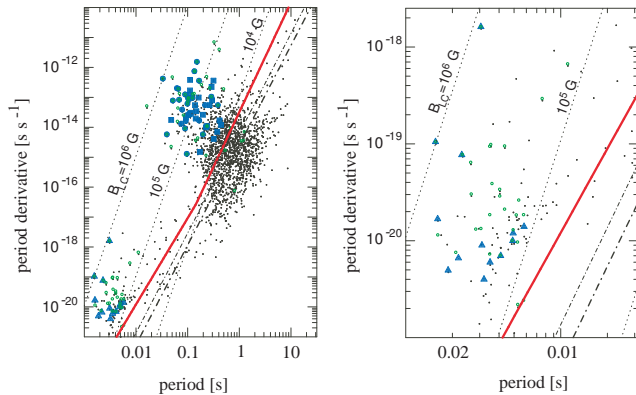


FIG. 2.— Outer-gap death line on the period versus period-derivative plane. The (red) solid line denotes the death line obtained in the present work. For comparison, previous outer-gap death lines are depicted as the thick and thin dash-dotted lines (Zhang et al. 2004). The thin dotted lines express the parameter region that gives the labeled magnetic-field strength, B_{LC} , at the light cylinder. The (blue) large points denote γ -ray detected pulsars, whereas the (green) small open circles denote X-ray detected pulsars (see text for details and references). *Left*: entire parameter space. *Right*: close up of millisecond parameter range.

Below the death line, or equivalently in the so-called ‘death valley’, the OG activity ceases. It follows that all the γ -ray pulsars detected so far and 84 (of 89) X-ray pulsars are located above the death line. The remaining five X-ray pulsars in the death valley, all of which are old nearby pulsars, will be discussed in § 4.2.

It also follows from figure 2 that the new constraint obtained by the pair-production threshold (§ 3) becomes important when we consider fast rotators ($P < 0.1$ s). To see this, the close-up figure of millisecond parameter range is presented as the right panel. It shows that all the X-ray and γ -ray millisecond pulsars (MSPs) are above the death line, including the marginal two cases (J1911-6000C in NGC 6752 and J0024-7204C in 47-Tuc). If the X-ray emission of such a marginal case is turned out to be thermal, it is probably due to the heated polar cap emission associated with OG activities. On the other hand, if they are non-thermal (as in the case of old, nearby, non-recycled pulsars), it may be due to a magnetospheric emission from the extended polar gap (see § 4.2).

4. DISCUSSION

It is found that the death line has a weak dependence on α . This is because negative feedback effects work (Hirotani 2006) in an OG and its electrodynamic structure little changes when we moderately change such parameters as α , P , and μ . However, the gap electrodynamic structure is mildly subject to change when we adopt different kT (eqs. [29] & [30]), because it directly affects the efficiency of γ - γ pair production.

In their death line calculation, Zhang et al. (2004) did consider the γ - γ pair-production threshold and wrote down the fractional gap thickness, f , as a function of α , P , \dot{P} , and r . In this paper, instead of using f , we considered two conditions ($N_{\gamma}\tau > 1$ and pair-production threshold) to find that the latter condition gives a tighter constraint for MSPs. The difference becomes particularly important when we investigate potential MSPs in globular clusters, which provide an efficient way to observe less-luminous MSPs with long exposures.

4.1. Death line of millisecond pulsars

For slowly rotating pulsars ($P > 0.1$ s), the OG is active if the magnetic field strength at the light cylinder, B_{LC} , is greater than 10^4 G. However, for MSPs ($P < 0.01$ s), the OG has enough luminosity only when $B_{\text{LC}} > 10^5$ G. The reasons are twofold: lower PC temperature and soft curvature spectrum. For the PC temperature, equation (35) gives $kT_{\text{max}} \propto B_{\text{LC}}^{5/16} P^{11/16}$, where $B_{\text{LC}} \propto \dot{P}^{1/2} P^{-5/2}$ and $\mu \propto P^{1/2} \dot{P}^{1/2}$ are used. Therefore, for the same B_{LC} , the heated PC temperature decreases with decreasing P . For the curvature photon energy, equations (6) and (7) give $h\nu_c \propto B_{\text{LC}}^{3/4} P^{5/4}$. Therefore, the maximally possible curvature photon energy, $h\nu_c$, also decreases with decreasing P .

In spite of the facts above, we should notice here that the gap meridional thickness is self-regulated so that the pair multiplicity within the gap may be kept unity on average. Therefore, the curvature photon energy (or equivalently, the exponential-cutoff energy) little changes as the pulsar ages. This argument is valid until the pulsar approaches the death line, and will be discussed in a separate paper.

4.2. Old nearby pulsars in the outer-gap death valley

In figure 2, we plot the X-ray detected pulsars by small (green) open circles. It follows that several pulsars with longer periods ($P > 0.5$ s) are located in the ‘death valley’, which indicates that their OGs have already finished activity. They are B0823+26, B1133+16, J0108-1431, B0943+10, B0628-28, all of which are old non-recycled pulsars with characteristic ages around 10^7 years (Becker et al. 2004; Becker et al. 2005; Becker et al. 2006). Although the photon statistics are limited, B0823+26 and B0628-28 are found to show predominantly non-thermal spectra.

We consider that their non-thermal X-rays are emitted from the PC accelerator (or polar gap) extended into the higher altitudes along the magnetic field lines curving *toward* the rotation axis (Fawley et al. 1977; Scharlemann et al. 1978; Arons & Scharlemann 1979; Arons 1983). For a moderately inclined rotator, such ‘toward curvature’ field lines exist on the opposite side of the OG on the PC surface (e.g., in the magnetic azimuthal angle range between 105° and 220° in fig. 3 for $\alpha = 60^\circ$, measured counter-clockwise from the $+x$ direction). In another word, after the OG in the first and fourth quadrant ceases activity, the extended polar gap in the second and the third quadrant remains active to emit non-thermal X-rays or soft γ -rays with small luminosity. Since it is reasonable to assume a free emission of e^- ’s from the NS surface by E_{\parallel} (Arons 1981), there will be no ‘death lines’ for this kind of extended polar gap. The space-charge-limited flow of e^- ’s will be continuously accelerated outwards by a weak E_{\parallel} to emit curvature photons from X-ray to soft γ -ray energies, depending on the potential drop in this gap. The photons will be emitted into the direction $\theta < \alpha$ and $\pi - \theta < \alpha$, where θ denotes the photon propagation angle with respect to the rotation axis. For instance, the total emission solid angle becomes 2π if $\alpha = 60^\circ$. This corresponds to a modification of the original pair-starved polar-cap (PSPC) model attempted to apply to the ‘away curvature’ field

lines (Muslimov & Harding 2004a,b; Venter et al. 2009). This topic, a modified version of the PSPC model, will be discussed in a separate paper.

4.3. Heated polar cap of millisecond pulsars

Let us finally consider the relationship with X-ray observations. To this aim, we present the OG solution obtained for a typical millisecond pulsar parameter, $P = 10$ ms, $\dot{P} = 10^{-19}$ s s $^{-1}$, by applying the numerical technique described in Hirovani (2011). Since the solution close to the death line cannot be easily obtained by numerical analysis, we consider this set of (P, \dot{P}) , which is located relatively away from the death line (fig. 2). To consider a moderate case, we assume $\alpha = 60^\circ$. We present the solved κ , the created current density normalized by the typical Goldreich-Julian (GJ) value, $\Omega B/2\pi$ in the left panel of figure 3. It follows that the created current becomes super-GJ, $\kappa > \cos \alpha = 0.5$, in the leading side (in the first quadrant), whereas sub-GJ in the trailing side (in the fourth quadrant). This is because the inward γ -rays propagate towards the rotational direction due to the aberration of the photon propagation direction to preferentially materialize as pairs in the leading side. The created current concentrate near the last-open field line in the leading side, because the magnetic flux surface (i.e., a constant A_ϕ surface) has a negative extrinsic curvature (like the saddle or the inner surface of a doughnut) in the lower altitudes where pair production mainly takes place. The inward γ -rays preferentially propagate towards the lower magnetic colatitudes (i.e., towards the magnetic equator) to materialize as pairs near the last-open field line. This forms a striking contrast with two-dimensional calculation, which predicts that the created current peaks in the middle or higher magnetic colatitudes (i.e., away from the last-open field lines) in the gap (fig. 1 of Takata et al. 2008).

Using κ and the Lorentz factors of the in-falling e^- 's at the PC surface, we can compute the maximum attainable surface temperature using equation (35). The result is presented in the right panel of figure 3. The integrated PC X-ray luminosity becomes 3.4×10^{30} erg s $^{-1}$, whereas the magnetospheric γ -ray luminosity becomes 4.4×10^{32} erg s $^{-1}$. We should notice here that this figure does not represent the actual temperature distribution on the PC surface of a millisecond pulsar by any means. For a weak surface magnetic field ($B < 10^9$ G) of millisecond pulsars, the cyclotron energy is comparable or less than the Coulomb energy. Thus, we can expect more or less isotropic heat conduction on the surface of a millisecond pulsar. The high heat conduction of subphotospheric layers, where the in-falling plasmas' energy is released, allows the heat to propagate across the NS surface, resulting in a greater hot region than given in figure 3 (right) with decreasing temperature toward the rim of the heated region. Since there is no reliable calculation of the heat conduction on a NS surface, we simply present the maximum attainable temperature in this paper.

From the X-ray observations of several nearby field millisecond pulsars (see Pavlov & Zavlin 1997, Zavlin & Pavlov 1998, Bogdanov et al. 2007 for J0437-4715; Becker et al. 2000, Becker & Achenbach 2002, for J0030+0451; Zavlin 2007 for J2124-3358; Zavlin 2006 for

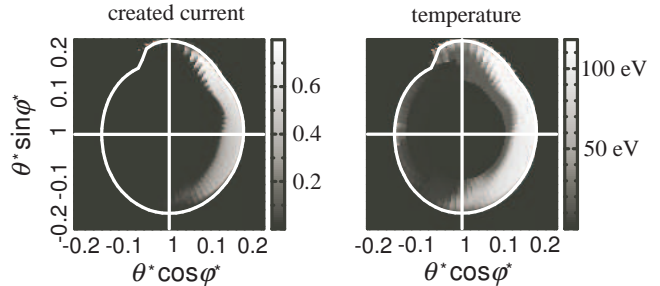


FIG. 3.— Solution of a self-consistent three-dimensional outer-gap for an example millisecond pulsar with $P = 10$ ms, $\dot{P} = 10^{-19}$ s s $^{-1}$, and $\alpha = 60^\circ$. Both the abscissa and the ordinate are in radian unit. The white curve denotes the foot points of the last-open magnetic field lines on the polar-cap (PC) surface. The magnetic field is assumed to be dipolar centered at the NS center. *Left:* Distribution of κ (eq. 20), or equivalently, the created current density normalized by the typical Goldreich-Julian value, $\Omega B/(2\pi)$ on the polar-cap surface. *Right:* Distribution of the maximum attainable temperature [eV] owing to the bombardment of the gap-accelerated electrons on the PC surface. Heat conduction in the trans-field direction is not considered.

J1024-0719), it is suggested that the heated PC emission can be fitted by a superposition of two thermal components. One component has a higher temperature around a few hundred eV with emission area of ~ 0.3 km 2 , which is sometimes referred to as the ‘core’ region of the heated PC. Another component has a lower temperature around 80 eV with emission area of ~ 30 km 2 , which is sometimes referred to as the ‘rim’ region of the heated PC.

We expect that the higher temperature region appearing in the leading side (i.e., in the first quadrant of figure 3) near the last-open field line corresponds to the observed core region, whereas the lower temperature region appearing in the trailing side (i.e., in the fourth quadrant) partially corresponds to the rim region. Although a detailed calculation of the heat conduction across the NS surface may not be easy, it is suggestive that the leading side tends to have a higher temperature than the trailing side. If the photon statistics will be improved in the future, the phase-resolved spectrum of a broad peak in the X-ray light curve will show a decreasing temperature with pulsar phase.

This work is supported by the Theoretical Institute for Advanced Research in Astrophysics (TIARA) operated under Academia Sinica and the National Science Council Excellence Projects program in Taiwan administered through grant number NSC 98-2752-M-007-006-PAE, and the Formosa Program between National Science Council in Taiwan and Consejo Superior de Investigaciones Científicas in Spain administered through grant number NSC100-2923-M-007-001-MY3.

5. APPENDIX

Derivation of equation (4) is given below. For simplicity, we assume a Newtonian dipole magnetic field configuration. We consider the plane (x, z) in which both the rotation and magnetic axes reside. Let us express the position of the cross section (point P1 in fig. 1) between the null surface and the last-open field line as (x_1, z_1) in Cartesian coordinates. Then, the radial distance of point

P1 from the NS center becomes

$$r_1 \equiv \sqrt{x_1^2 + z_1^2} = \varpi_{\text{LC}} \frac{\sin^2(\theta_{\text{null}} - \alpha)}{\sin^2(\theta_{\text{LC}} - \alpha)}, \quad (42)$$

where θ_{null} specifies the null surface, and θ_{LC} the colatitudes (measured from the rotation axis) of the point at which the last-open field line becomes tangent to the light cylinder. Thus, the distance of point P1 from the rotation axis becomes

$$x_1 = \varpi_{\text{LC}} \frac{\sin^2(\theta_{\text{null}} - \alpha)}{\sin^2(\theta_{\text{LC}} - \alpha)} \sin \theta_{\text{null}} \quad (43)$$

If a photon is emitted leftward from point P1, it crosses the critical field line (fig. 1) before escaping from the gap at point P2 (x_2, z_2). For a Newtonian dipole field, we obtain

$$r_2 \equiv \sqrt{x_2^2 + z_2^2} = \varpi_{\text{LC}} \frac{\sin^2(\theta_2 - \alpha)}{\sin^2(\theta_{\text{null}} - \alpha)}, \quad (44)$$

and hence $x_2 = r_2 \sin \theta_2$. Therefore, we obtain the distance between P1 and P2,

$$x_1 - x_2 = r_1(\sin \theta_{\text{null}} - \tan \theta_2 \cos \theta_{\text{null}}) \quad (45)$$

For photons emitted from the middle colatitude in the gap, we thus obtain the propagation distance below the critical field line,

$$l \approx \frac{x_1 - x_2}{\sqrt{2}} = \frac{r_1}{\sqrt{2}}(\sin \theta_{\text{null}} - \tan \theta_2 \cos \theta_{\text{null}}) \quad (46)$$

where

$$\frac{\cos \alpha \tan \theta_2 - \sin \alpha}{1 + \tan^2 \theta - 2} = \frac{\cos \theta_{\text{null}} \sin^4(\theta_{\text{null}} - \alpha)}{\sin^2(\theta_{\text{LC}} - \alpha)} \equiv \epsilon. \quad (47)$$

The factor $\sqrt{2}$ in the denominator of equation (46) is appropriate if the poloidal magnetic field lines are co-centric. For a dipole field geometry on the poloidal plane, equation (46) overestimates l . Nevertheless, the inward γ -rays propagate towards the leading side in a three-dimensional magnetosphere owing to aberration and propagate a longer distance than what is evaluated only on the poloidal plane. Thus, equation (46) gives a good estimate. Since $\epsilon \ll 1$, $\tan \theta_2 \approx \tan \alpha$ reduces equation (46) into equation (4).

REFERENCES

- Abdo, A. A. et al. 2010a, *ApJS*, 187, 460
 Abdo, A. A. et al. 2010b, *ApJ*, 712, 957
 Abdo, A. A. et al. 2010c, *ApJ*, 714, 927
 Aliu, E. et al. 2008, *Science* 322, 1221
 Arons, J. 1981, *ApJ* 248, 1099
 Arons, J. 1983, *ApJ* 302, 301
 Arons, J., Scharlemann, E. T. 1979, *ApJ* 231, 854
 Bassa, C. G. et al. 2004, *ApJ*, 609, 755
 Bogdanov, S. et al. 2006, *ApJ*, 646, 1104
 Bogdanov, S. et al. 2007, *ApJ*, 670, 668
 Bogdanov, S. et al. 2010, *ApJ*, 709, 241
 Bogdanov, S. et al. 2011, *ApJ*, 730, 81
 Bogdanov, S. and Grindlay, J. E. 2009, *ApJ*, 703, 1557
 Becker, W. et al. 2000, *ApJ*, 545, 1015
 Becker, W., & Achenbach, B. 2002, in *Neutron Stars, Pulsars, and Supernova Remnants*, Eds. Becker, W., Lech, H., Trümper, MPE-Report 278, p. 64
 Becker, W. et al. 2003, *ApJ*, 594, 798
 Becker, W. et al. 2004, *ApJ*, 615, 908
 Becker, W. et al. 2005, *ApJ*, 633, 367
 Becker, W. et al. 2006, *ApJ*, 645, 1421
 Becker, W. 2009, in *Neutron Stars and Pulsars*, Eds. Becker, W., *Astrophysics and Space Science Library* 357, p. 91
 Becker, W., Trümper, J. 1999, *A&A*, 341, 803
 Cheng, K. S., et al. 1986a *ApJ*, 300, 500
 Cheng, K. S., et al. 1986b *ApJ*, 300, 522
 Cheng, K. S. et al. 2000, *ApJ*, 537, 964
 D'Amico, N. et al. *ApJ*, 570, L89
 Elsner, R. F. et al. 2008, *ApJ*, 687, 1019
 Fawley, W. M., Arons, J., & Scharlemann, E. T. 1977, *ApJ* 217, 227
 Frackowiak, M., Rudak, B. 2005, *ApJ Adv. Space Res.*, 35, 1152
 Grindlay, J. E. et al. 2002, *ApJ*, 581, 470
 Grindlay, J. E., Bogdanov, S. 2009, in *Neutron Stars and Pulsars*, Eds. Becker, W., *Astrophysics and Space Science Library* 357, p. 165
 Goldreich, P. Julian, W. H. 1969, *ApJ*. 157, 869
 Guillemot, L. et al. arXiv:1101.0669
 Halpern, J. P. et al. 2008, *ApJ* 688, L33
 Harding, A. K. et al. 2005, *ApJ*, 622, 531
 Heinke, C. O. et al. 2006, *ApJ*, 651, 1098
 Hirotani, K. 2006, *ApJ* 652, 1475 (H06a)
 Hirotani, K. 2006, *Mod. Phys. Lett. A (Brief Review)* 21, 1319–1337 (H06b)
 Hirotani, K. 2008, *ApJ* 688, L25
 Hirotani, K. 2011, submitted to *ApJ*.
 Keith, M. J. et al. 2011, arXiv:1102.0648
 Kuiper, L. et al. 2000, *A&A* 359, 615
 Kuiper, L. et al. 2002, *ApJ*, 577, 917
 Mineo, T. et al. 2000, *A&A*, 355, 1053
 Muslimov, A. G., & Tsygan, A. I. *MNRAS*, 255, 61
 Muslimov, A. G., & Harding, A. K., 2004a, *ApJ*, 606, 1143
 Muslimov, A. G., & Harding, A. K., 2004b, *ApJ*, 617, 471
 Pellizzoni, A. et al. 2009, *ApJ* 695, L115
 Pilia, M. et al. 2010, *ApJ* 723, 707
 Pilia, M. & Pellizzoni, A. 2011, arXiv:1101.2125
 Pavlov, G. G., Zavlin, V. E. 1997, *ApJ*, 490, L91
 Romani, R. W. 1996, *ApJ*, 470, 469
 Romani, R. W., & Watters, K. 2010, *ApJ* 714, 810
 Saito, Y. et al. 1997, *ApJ*, 477, L37
 Saz Parkinson, P. M. et al. 2010, *ApJ*, 725, 571
 Saz Parkinson, P. M. et al. 2011, arXiv:1101.3096
 Scharlemann, E. T., Arons, J., & Fawley, W. T., 1978 *ApJ*, 222, 297 (SAF78)
 Takata, J. et al. 2008, *MNRAS* 386, 748
 Venter, C. et al. 2009, *ApJ* 707, 800
 Zavlin, V. E., Pavlov, G. G., 1998, *A&A*, 329, 583
 Zavlin, V. E. 2002, *ApJ*, 569, 894
 Zavlin, V. E. 2006, *ApJ*, 638, 951
 Zavlin, V. E. 2007, *Ap&SS*, 308, 297
 Zhang, L. et al. 2004, *ApJ* 604, 317